BROAD BAND, HIGH RESOLUTION SPECTROSCOPY OF HIGHLY CHARGED IONS WITH A MICROCALORIMETER ON AN ELECTRON BEAM ION TRAP

E. SILVER, H. SCHNOPPER, S. BANDLER, N. BRICKHOUSE AND S. MURRAY
Harvard-Smithsonian Center For Astrophysics

M. BARBERA
Osservatorio Astronomico G.S. Vaiana

E. TAKACS
Massachusetts Institute of Technology

J. D. GILLASPY, J. V. PORTO, I. KINK, AND L. HUDSON
National Institute of Standards and Technology

J. M. LAMING
Naval Research Laboratory

N. MADDEN, D. LANDIS, J. BEEMAN AND E. E. HALLER
Lawrence Berkeley National Laboratory

RHEINHOLD SCHUCH
University of Stockholm

The behavior of exotic highly charged ions can be studied spectroscopically in an Electron Beam Ion Trap (EBIT). The EBIT produces customized, well-characterized, homogeneous plasmas for a wide variety of precision measurements. It is uniquely capable of simulating astrophysical plasma conditions to systematically examine how the atomic structure and dynamics of plasma ions influence the energy release in cosmic x-ray sources. The EBIT can also be used to study the creation of exotic *hollow atoms*. We report on measurements made a broad band high resolution microcalorimeter.

1 Introduction

Highly-charged ions are exotic and exceedingly rare on Earth. Yet, on a cosmological scale, the physics of highly charged ions dominates the nature of the universe[1]. Increasing interest in studying such ions has been motivated by several factors: (1) the advent of improved methods to produce them in a small-scale laboratory environment under well-controlled conditions suitable for spectroscopic study (e.g., Electron Beam Ion Trap, (EBIT)), (2) the dawn of the age of high-precision x-ray astrophysics (with the launch of powerful new x-ray telescopes), (3) the desire to understand the detailed electronic structure of atoms, particularly as it relates to the fundamental nature of space and time described by quantum electrodynamics and many-body relativity theory, and (4) the hope of discovering new applications which may form the basis for advanced technologies of the future.

X-ray spectroscopy is one of the primary ways used to study the physics of highly charged ions. High

resolution x-ray crystal spectrometers and broad band semiconductor ionization detectors have been the traditional tools for these investigations. The spectra obtained with these instruments furnish measurements of atomic energy levels, ionization energies, excitation cross-sections and recombination rates. Although they have yielded many excellent results [2,3] these instruments are limited either by a poor energy resolution (solid state detector) or by a low efficiency and a narrow bandwidth (crystal spectrometer). These limitations make it difficult at times to obtain results with the absolute accuracies required for direct comparison with theory.

Faced with similar problems, the x-ray astronomy community embarked on the development of cryogenic x-ray microcalorimeters 15 years ago. The most important performance goals have been finally achieved. Several groups [4,5,6,7] can demonstrate microcalorimeters with high resolving power, quantum efficiency approaching 100% and a bandwidth that spans 0.1-10 keV. In a microcalorimeter (operating at~ 65 mK), absorbed x-ray photons are converted into heat that causes a temperature rise proportional to the x-ray energy. The theoretical energy resolution is independent of photon energy and, depending upon the exact details of the instrument, can be less than 1 eV [8].

No longer a laboratory curiosity, these new spectrometers are being used for a wide range of scientific and industrial applications. Microcalorimeters have been flown on two successful sounding rockets to study the soft x-ray background [9], they have provided unprecedented capabilities in materials analysis [10,11], particle physics [12] and mass spectroscopy [7]. We can now add fundamental studies of exotic ions to the list[13,14,15] and here we report on our recent measurements with a microcalorimeter on the EBIT at the National Institute of Standards and Technology (NIST). Here we report on broad band, high resolution measurements of single charge states of astrophysically relevant ionic species . They have led to improved precision of excitation cross-section determinations and relative line intensities and in turn can provide accurate temperature and density diagnostics of hot astrophysical plasmas. We also present preliminary results from experiments designed to study the neutralization and relaxation of highly charged ions at solid surfaces by measuring x-ray spectra from several steps in the recombination cascade.

2 Laboratory Astrophysics

X-ray spectroscopic measurements are used to determine the temperature distribution, density, ionization state, and elemental composition of hot cosmic plasmas. Knowledge of these basic parameters provides an understanding of physical processes in the hot universe such as atmospheric heating, transport, shock waves and accretion. Plasmas of special interest are found in the magnetically heated coronae of late-type stars, the accretion disks surrounding collapsed stellar objects, the bubbles of gas heated by supernovae and the tunnels throughout interstellar space that they create, the halos of elliptical galaxies, the nuclei of active galaxies and the vast regions in galaxy clusters. The determination of the physical parameters that

define the plasma relies on complex models of the continuum and line emission. The atomic data for these models are largely derived from theoretical work. In rare cases, appropriate laboratory data may be available.

The current understanding of the fundamental processes occurring in highly ionized plasmas is not commensurate with the quality of data obtained by the new X-ray telescopes and spectrometers flown on ASCA, Chandra and XMM-Newton. Few individual atomic rates are known with an accuracy less than 20% and emission lines that depend on many processes (e.g. both direct excitation and cascades from recombination) are less accurately known. Dielectronic recombination rate coefficients and the ionization balances derived using them can also be uncertain by factors of two or more.

Plasma emission models of X-ray spectra now compute several million emission lines for the cosmically abundant elements. Many processes can contribute to the population of the energy level producing an observed transition. While measurements of cross sections for single atomic processes are invaluable, the sheer numbers of such processes and the range of energies under which these processes occur make it impractical to attempt more than a few carefully selected experiments. Efforts to benchmark the plasma spectral models by using only the astrophysical data have led to a growing recognition that the models are not only inaccurate, but are also incomplete.

To achieve the best scientific interpretation of the data from Chandra, XMM-Newton and ASCA, theoretical calculations must be verified or modified by the results obtained from spectroscopic measurements in the laboratory. An excellent way to study the behavior of highly charged plasma ions is to confine them in an Electron Beam Ion Trap (EBIT). The EBIT produces customized, well-characterized, plasmas suited to a wide variety of precision measurements. The manipulation of the plasma conditions in the EBIT can be used to generate a comprehensive data base for comparison with theoretical atomic physics calculations. The EBIT is also uniquely capable of simulating specific slices through astrophysical

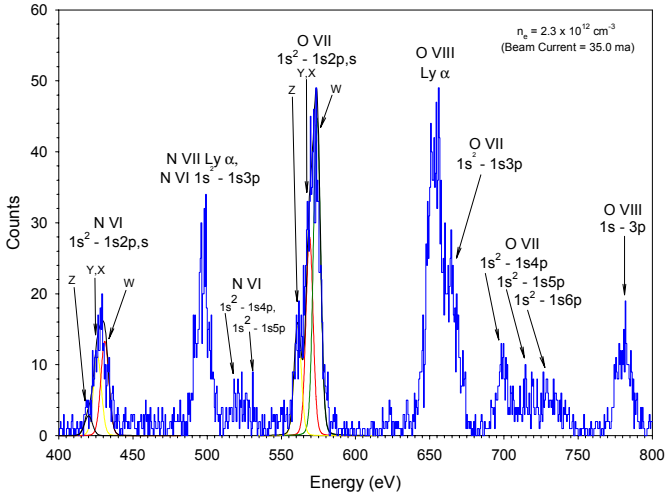

Figure 1. Microcalorimeter X-Ray spectra from collisionally excited ions of nitrogen and oxygen from the NIST EBIT. The contributions to He-like nitrogen (N VI) and He-like oxygen (O VII) from the forbidden line (Z; dark blue), intercombination line (Y,X; red) and resonance line (W; dark green) are shown. The collection time was ≈ 30 min (from Silver et al. [13]).

plasma conditions (ions at rest, electrons with nearly constant energy). This allows the systematic examination of how the atomic structure and dynamics of plasma ions influence the energy release in cosmic X-Ray sources. The literature contains numerous examples of EBIT applications [16,17]. Measurements of impact excitation rates, excited state lifetimes, ionization cross sections, resonant excitation and dielectronic recombination cross sections and precision wavelength measurements.

2.1 EBIT Spectroscopy With A Microcalorimeter

Operating at 65 mK, our microcalorimeters combine excellent energy resolution with relatively high count rate performance and large collecting area in the 0.1 to 10 keV energy band. In the calorimeter, x-ray photons are absorbed in a foil of superconducting tin and converted into heat. The temperature rise is proportional to the x-ray energy and is measured with a neutron transmutation-doped (NTD) germanium thermistor that is attached to the underside of the absorber. The small heat capacity of the composite calorimeter produces a relatively large temperature change. The NTD thermistor is impedance-matched to a JFET negative voltage feedback circuit [9, 10 and references therein]. The detector was designed for broad band applications and provides 95% quantum efficiency at 6 keV. Its dimensions are 0.4 mm x 0.4 mm x 7 μm. Our most recent detectors have an energy resolution of 4.8 eV across the energy band of 0.25 to 7 keV.[4] The measurements discussed here were made by detectors with 6 eV.

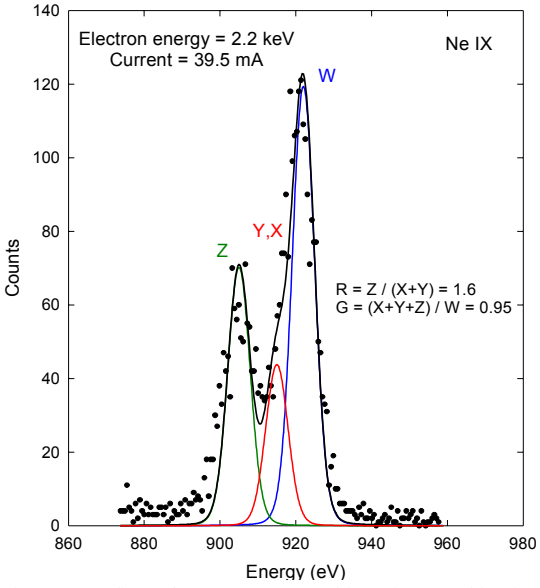

Figure 3. A fit to the resonance (W; blue), intercombination (X,Y; red) and forbidden (Z; dark green) lines yields a line ratio R= Z/(X+Y) = 1.6 and G = (X+Y+Z)/W =0.95. The collection time was 29 min (from Silver et al. 2000).

2.2 Diagnostics Common to Astrophysical and Laboratory Plasmas

The grating spectrometers on XMM-Newton and Chandra have maximum sensitivity for the wavelength range of 35-5 Å (0.3 - 2.5 keV), the region where most cosmic X-ray sources emit copiously from L shell transitions in Fe. This energy band also includes numerous K shell transitions from H- and He-like ions of N, O, Ne, Mg, and Si . The H- and He-like ions of heavier elements such as S, Ar, Ca, Fe, Ni are

prominent in spectra taken with CCD detectors at energies between 2 and 7 keV, albeit at a lower energy resolution.

The importance of He-like diagnostics obtained from ions of C through Fe cannot be overstated. The intercombination, forbidden, and resonance lines provide density and temperature diagnostics over a wide range of parameters in both photoionized and collisionally ionized plasmas. The He-like ions N VI, O VII, Ne IX and Mg XI are especially important diagnostic line ratios for the electron density and are widely used in X-Ray astronomy. These lines are easily identified in spectra and are unblended (Ne IX lies close to lines of Fe XIX, but can be resolved with the Chandra gratings). N VI and O VII lines are density sensitive above 10^{10} cm^{-3} while Ne IX and Mg XI are useful from 10^{11} - 10^{12} cm^{-3}. O VII densities in this range have been observed only in solar flares[18]. These density ranges are well matched to the electron density that can be obtained in the EBIT electron beam (up to ~5×10^{12} cm^{-3}).

Although theoretical calculations for He-like ions are generally believed to be reasonably accurate, they have not all been benchmarked with experimental results. For example, line ratios obtained from early Chandra grating spectra suggest that there are inconsistencies with electron density diagnostics that should be resolved with laboratory measurements. A 20 % uncertainty in the line ratio may be critical. Laboratory measurements made under controlled conditions that will yield line ratios to a few percent accuracy and sample an order of magnitude in electron density over the range where the line ratio changes steeply are required. An initial step in this direction has been made recently by successfully producing all the lines at a single density and then obtaining line ratios consistent with this [4]. Figure 1 shows the He-like and H-like (Lyman α) transitions of nitrogen (N VI and N VII) and oxygen (O VII and O VIII) along with some higher transitions ($1s^2$ -1snp; n> 2) measured with our microcalorimeter on the NIST EBIT. The relative contributions of the resonance (W; dark green), intercombination (X,Y; red) and forbidden (Z; dark blue) lines to the He-like emission of nitrogen and oxygen are determined from a least squares fit (solid black line) to the data (blue histogram) using a nominal detector

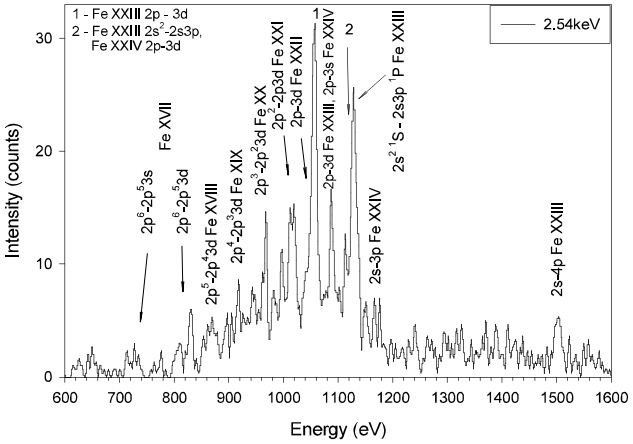

Figure 3. Section of a microcalorimeter spectrum of Fe L lines recorded at an EBIT electron energy of 2.54 keV.Lines of Fe XVII - Fe XXII are prominent.

energy resolution of 6 eV. The ratio of the forbidden to intercombination lines was consistent with an electron density of 5×10^{11} cm $^{-3}$. Similarly, Figure 2 shows a measurement from the EBIT of the helium-like complex in Ne IX. The contributions from the resonance, intercombination and forbidden lines are clearly seen and the R value [19] for Ne IX was also consistent with a density of 5×10^{11} cm $^{-3}$.

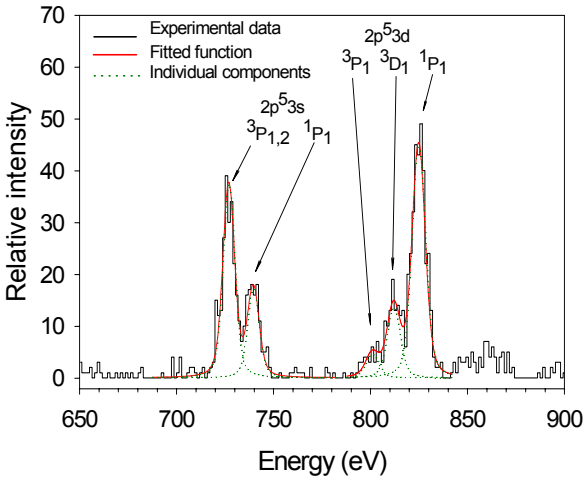

Figure 4. Fit to the six strong Fe XVII lines recorded at an electron beam energy of 900 eV. The wavelengths are 15.014, 15.265, 15.456, 16.780, 17.055 and 17.100 Å . The last two are blended together at the resolution of the microcalorimeter, and are fitted as one component.

2.3 L Shell Spectra

Fe ions from Li-like to Ne-like exhibit prominent transitions from n=3 or higher levels to the n=2 level. The greater number of x-ray emitting levels available in each ion cause these spectra to be considerably more complex than K-shell spectra. The strongest lines have been observed previously and identified in solar flares [20,21]. Although the configuration of many of the weaker lines is unknown, it will be necessary to work with these weaker lines for many astrophysical applications. For example, the measurement of electron densities or elemental abundances relative to Fe will, in general, require the identification of a weak line (density sensitive Fe for a density diagnostic or density insensitive from Ni or other element for a relative abundance measurement) against the *background* of other weak Fe lines. A substantial amount of work on line identifications in the Fe L-shell complex has already been done using a crystal spectrometer on an EBIT [22,23], but most of the diagnostic potential of these lines remains to be verified.

Table 1. Fe XVII Line Ratios Relative to 15.012 Å

Wavelength Å	Data (900eV)	Distorted Wave	R-Matrix	Capella	HR 1099
15.265	0.34 ± 0.02	0.25	0.25	0.38	0.46
15.456	0.10 ± 0.01	0.047-0.036	0.059-0.046	0.07	0.08
16.780	0.45 ± 0.04	0.46 - 0.41	0.47-0.41	0.63	0.57
17.055 + 17.100	0.88± 0.90	0.88 - 0.77	1.03-0.91	1.36	1.47

* Laming et al. 2000

Two representative spectra of Fe L emission obtained with the microcalorimeter are shown in Figures 3 and 4. Each spectrum was obtained at a different electron excitation energy while the electron beam

current remained fixed. Figures3 and 4 are records of the emission produced by electrons with excitation energies of 2.5 keV and 0.9 keV, respectively. It only required 20 min to record each spectrum.

2.4 Fe XVII Line Ratios

We have recently published new observations of emission line intensity ratios of Fe[15] . The observations are compared with collisional-radiative models using atomic data computed in distorted wave and R-matrix approximations, which follow the transfer of the polarization of level populations through radiative cascades. While we refer the reader to the publication for details of the measurements and calculations we review some of the results. Table 1 , partly reproduced from Laming et al., shows the Fe XVII line intensity ratios for a beam energy of 900 eV. The range of theoretical ratios extends from results calculated in the limit of zero polarization to those in the limit of maximum polarization. The finite distribution of pitch angles in the electron beam causes the true theoretical result to lie somewhere in between these two limits. The polarization correction required for the microcalorimeter is always smaller than that for a crystal spectrometer, but it remains the dominant systematic uncertainty in our experiment at these two beam energies. Our results for the intensity ratio of the 15.014 line to the 15.265 line are 2.94 +/- 0.18 and 2.50 +/- 0.13 at beam energies of 900 and 1250 eV, respectively. As shown in Table 2 and Laming et al. [15], these results are not consistent with the theoretical expectations of the collisional-radiative models which predicted the line at 15.014 to be stronger than what is actually observed in the laboratory, in observations by Chandra of Capella [24] and HR 1099 (available through the NASA Emission Line Project) and spectra obtained from the sun. Prior to these

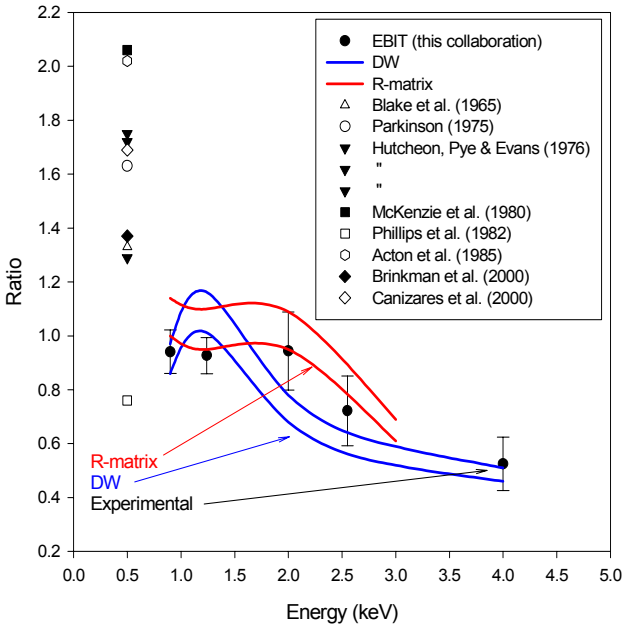

Figure 5. The intensity ratio ($I_{16:780} + I_{17:055} + I_{17:100}$)= ($I_{15:014} + I_{15:265} + I_{15:456}$) vs electron beam energy. (Laming et al. 2000). The first three lines originate in the $2p^5$ 3s configuration and the second three in the $2p^5$ 3d. Also, model calculations using the distorted wave results (Bhatia & Doschek , 1992) and where appropriate the R matrix results of Mohan, Sharma, & Eissner (1997) are overlaid. The *upper* and *lower* curves are for unpolarized and completely polarized emission, respectively. The observational ratios from various solar and stellar observations are shown for reference on the same plot. For these, the energy scale on the x-axis should be disregarded. Fe XVII is generally formed in plasmas at a temperature of 5×10^6 K, and electrons with energies close to threshold, i.e. < 1 keV dominate the excitation rate.

laboratory measurements, the discrepancies between the theory and astronomical observations led to suggestions that resonance scattering removes photons predominantly from the line of sight in this transition [20,25,26]. Our EBIT/ microcalorimeter results support conclusions from earlier EBIT work with crystal spectrometers at the LLNL [23] that the degree of resonance scattering in the solar 15.014 line has been overestimated in previous analyses of astrophysical data.

Our microcalorimeter measurements have gone beyond previous experiments with crystals. We have assessed the intensity ratio of the three lines between the $2p^6$-$2p^5 3s$ configurations to the three lines between the $2p^6$-$2p^5 3d$ configurations. Figure 5 shows the intensity ratios from our data for the lines originating from the $2p^5 3s$ to those from $2p^5 3d$. For electron excitation energies greater than 1.25 keV they are obtained by summing the number of detected photons over the spectral regions where the $2p^6$-$2p^5 3s$ and $2p^6$-$2p^5 3d$ lines appear. Details may also be found in Laming et al. [15]. Both the R-matrix and distorted wave approximations shown in the Figure 5 agree with each other and our experimental results much better than they agree with most solar and stellar observations. The basic electron impact excitation theory for these lines in Fe XVII appears to be correct, in contrast with that for the 15.265/15.014 ratio and other processes not present in our experiment must play a role in forming the Fe XVII spectrum in solar and astrophysical plasmas.

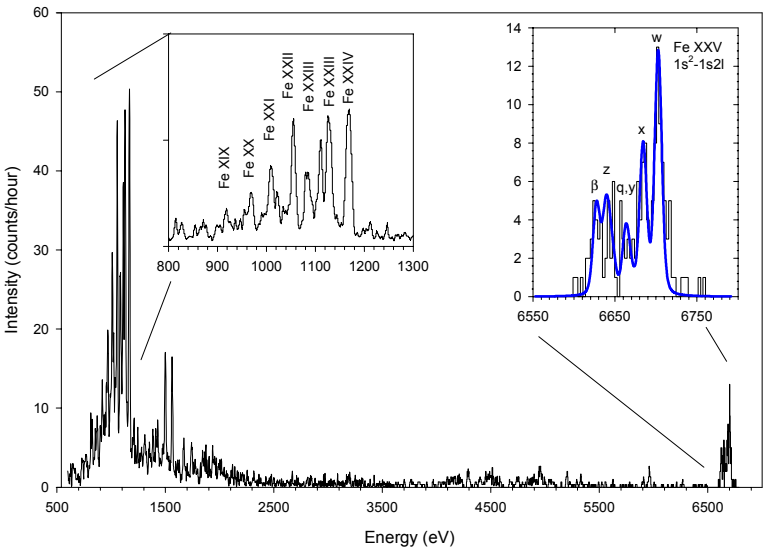

Figure 6. Simultaneous L and K spectra from Fe obtained with the microcalorimeter. The inset at the upper left shows the richness of the Fe L emission and the inset at the upper right the He-like Fe XXV complex and Fe XXIV satellites.

2.5 Electron Temperature

An accurate assessment of temperature diagnostics is vital to the astrophysics of plasmas where collisionless heating occurs. Solar/stellar coronae and flares, supernova remnants, clusters of galaxies, comets and presumably many related phenomena are examples. Collective plasma motions complicate any

theoretical treatment. Electron temperature diagnostics from a single ionization state are potentially more accurate than temperatures derived from ionization balance calculations (which generally rely on the relative line intensities of adjacent charge states and the assumption of ionization equilibrium). The microcalorimeter has this capability to observe a wide spectral region with high resolution simultaneously and therefore allows us to study, for example, the L shell spectrum and K shell inner satellites in ions such as Fe XVII - Fe XXIV. The Fe K and L lines sample the same local electron temperature, whereas the shape of the continuum emission spectrum provides an accurate estimate of the average electron temperature of a stellar corona. These lines will be observed with Chandra and XMM-Newton.

The energies of the Fe K lines (6.4 -6.7 keV) and the Fe L lines (about 1 keV) fall easily within the bandpass of the calorimeter as shown in Figure 6. The inset in the Figure is an expanded view of the richness of the low energy L spectra and the high energy He-like K spectra. The correlation between the line intensity ratio and the EBIT electron beam energy can be used to determine the relationship between line ratio and electron temperature (or distribution function in the case of extreme departures from equilibrium).

2.6 Measurement of Electron Impact Excitation Cross-Sections

The temperature dependent behavior of electron-impact excitation cross-sections is key to the sensitivity of a subset of the diagnostics discussed above. As we have shown for the Ne-like Fe XVII lines, discrepancies exist between theoretical predictions of the intensity ratios of the strongest lines and the experimental observations. We are addressing this important problem by taking advantage of the broad band capability of the microcalorimeter (200 eV to 10 keV) to observe simultaneously emission lines and radiative recombination (RR) features onto the same charge state. Since cross sections for the RR transitions can be calculated to high precision [2], the relative intensity ratios between the emission lines and the RR lines provide absolute excitation cross sections and line intensities.

To demonstrate this new capability, we have made pilot measurements on Ne-like Kr XXVII. Figure 7 shows the main features of the spectrum. The x-ray energy range of interest covers 1.5 keV to 4 keV. The strongest Ne-like Kr emission lines appear between 1.6 and 2.2 keV and are labeled by 3s and 3d. Apart from these n=3 to n=2 transitions, lines from higher lying levels (n= 4, 5, 6, ...) are also observed all the way up to the n=2 series limit as shown in the inset. Above this limit only recombination features are observed where the energies of the lines correspond to the sum of the binding energy of the bound state level in which the electron is captured and the energy of the free electron from the EBIT electron beam. The highest energy (close to 4 keV) and most separated RR feature corresponds to RR captures onto the n=3 level.

The energy of the electron beam was determined by fitting the set of RR features above the series limit

of the n=2 bound transitions by leaving the energy of the electron beam a free parameter. The strongest features in the spectra are Kr XXVII n=3 to n=2 lines that have been identified in one of our earlier experiments [14] . The 3s and 3p lines at around 1650 eV and 1705 eV x-ray energy consist of different components. The relative ratios between these components were fixed to the theoretical value obtained from HULLAC calculations. At the low energy shoulder of the Kr XXVII lines there are weak satellite contributions from Kr XXVI and are accounted for in determining the line intensity. The intensities of the 3d and 3s transitions were determined from curve fits and will be compared to the intensity of the n=3 RR lines to obtain the experimental cross section ratios [27].

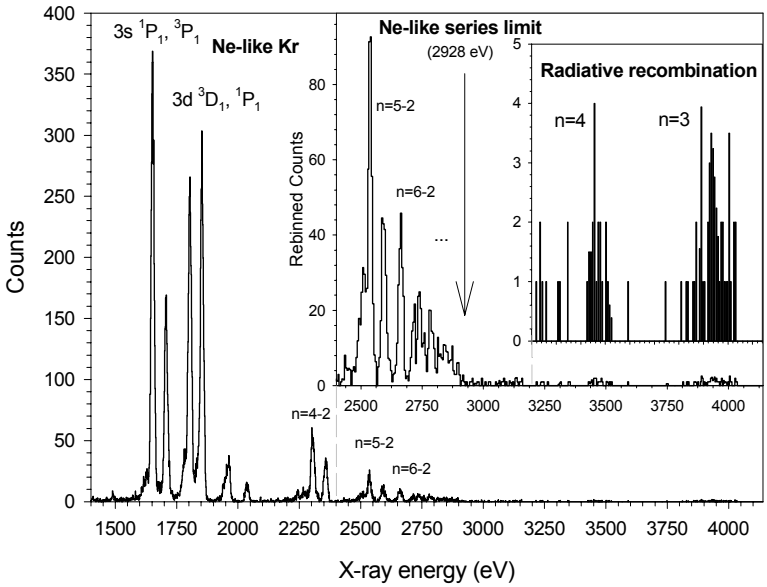

Figure 7. Microcalorimeter spectrum of Kr XXVII in the EBIT. The strongest Ne-like lines appear are labeled by 3s and 3d. Lines from higher lying levels (n= 4, 5, 6, ...) are also observed, up to the n=2 series limit. Above this limit only recombination features can be observed. The highest energy RR feature corresponds to captures into the n=3 level

3 EBIT Surface Physics With a Microcalorimeter

The processes that dictate the neutralization of slow, highly charged ions as they approach and penetrate the surface of a metal have fundamental interest [28,29]. Generally, it is believed that highly charged ions efficiently capture a large number of electrons into high quantum states. The ionic configuration is termed a "hollow atom" - one with virtually an empty core surrounded by electrons occupying high Rydberg levels. The extreme population inversion produced in these ion-surface interactions has the potential to be exploited for x-ray laser schemes if a highly dense plasma could be produced against a metal surface.

The dynamics of the decay of these hollow atoms depend strongly on their velocity. Slow ions generally decay via Auger , x-ray and UV transitions before they reach the first atomic layer of the surface, while fast ions neutralize via bulk interactions beneath the surface. Insights into these mechanisms are obtained from measurements of electron and photon emission spectra as a function of incident ion velocity.

In an experiment to followup work done previously by several of these authors [30], we directed Ar^{17+} ions with a velocity of ~8 × 10^7 cm/s into the polyimide window attached to the liquid nitrogen shield of the cryostat (see Figure 8). The microcalorimeter spectrum from the recombining Ar^{17+} ions is shown in Figure 9. The argon Kα and Kβ,γ complex are clearly distinguished. The inset in Figure 9 is an expanded view of the Ar Kα showing the contributions from transitions KL^1 and KL^8. The spectrum in red , (overlayed in arbitrary units for comparison of shape only) was obtained with crystal spectrometers by Briand et al. [31] that indicates that the relative intensities of the individual transitions is different in the two measurements. The investigations with the microcalorimeter will continue so that the discrepancies can be understood.

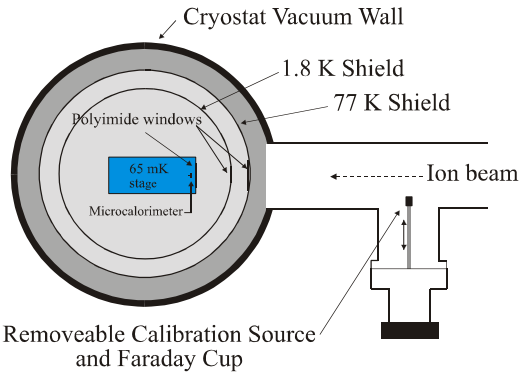

Figure 8 A schematic view of the internal geometry of the microcalorimeter and cryostat

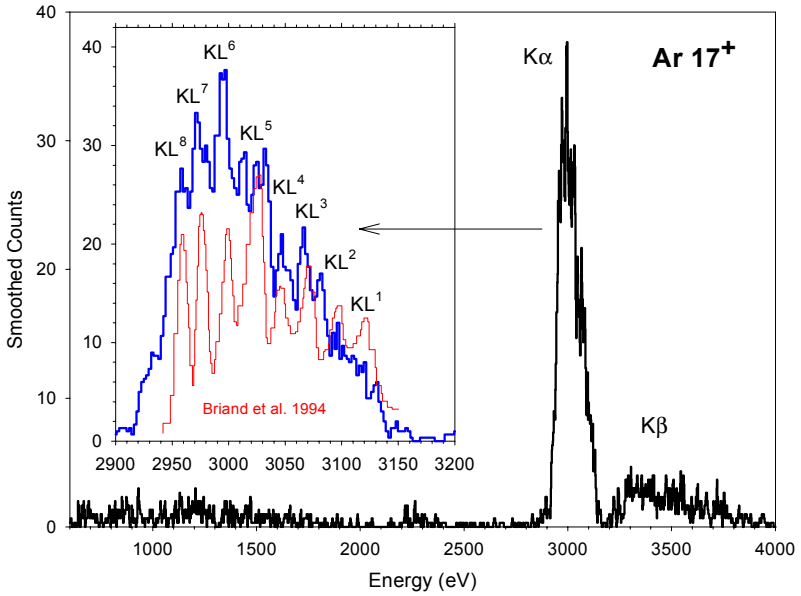

Figure 9 The microcalorimeter spectrum obtained from Ar^{17+} ions as they struck a polyimide window with a velocity of 8 × 10^7 cm/s.The Ar Kα and Kβ,γ complex is evident. The inset shows the expanded view of the individual transitions within the Ar Kα (blue). The red spectrum is the spectrum from Briand et al. Made with a crystal spectrometer. It is overlayed with arbitray units to compare the shape and relative intensities between the two measurements.

References

1. Mokler, *The Forward*, Physica Scripta, **T80A**, 3 (1999)

2. P. Beiersdorfer et al., *Phys. Rev. A*, **46**, 7, 3812 (1992)

3. G.V. Brown et al., *Ap. J.* , **502**,1015 (1998)

4. E. Silver et al., To appear in proceedingds of *the 9th International Workshop on Low Temperature Detectors,* August 2001.

5. C.K Stahle. et al, *SPIE* (1999)
6. A. Alessandrello et al., *Phys. Rev. Lett*., **82** 513 (1999)
7.Friedrich, et al. *Nuclear Instruments and Methods in Physics Research (Section A)* (2000)
8. S.H Moseley et al., *J. Appl. Phys*. **56**, 1257 (1984)
9. F.S Porter et al. , *Nuclear Instruments and Methods in Physics Research (Section A)* (2000
10. D. Wollman et al., *Nuclear Instruments and Methods in Physics Research (Section A)* (2000)
11. E. Silver et al., *X-ray Spectrometry*, **25,** 265 (1997)
12. B. Sadoulet , *Nuclear Instruments and Methods in Physics Research (Section A)*, (2000)
13. E. Silver et al., *Ap. J*., **541**, 495 (2000)
14. I. Kink et al., *Phys Rev E*. to be published (2001)
15. M. Laming et al., *Ap.J*., **545**, L161(2000)
16. P. Beiersdorfer et al., *Hyperfine Interactions*, 99: (1-3) 203-215 (1996)
17. J.D. Gillaspy, *Physica Scripta*, T65, 168 (1996)
18.G. A. Doschek, et al., *ApJ*, **249**, 372 (1981)
19. Gabriel, A.H., and Jordan, C., in *Case Studies in Atomic Collisions Physics*. (McDaniel, E.W., McDowell, M.R.C., eds.) North Holland, Amsterdam, **2**, 211 (1972)
20. K. J. H. Phillips et al., *ApJ*, **256**, 774 (1996)
21. K. J. H. Phillips et al., *A&AS*, **138**, 381 (1999)
22. G. V. Brown, et al. (1999)
23. G.V. Brown et al., *Ap. J.* , **502**,1015 (1998)
24. A. C Brinkman et al., *Ap. J.*, **530**, L111 (2000)
25. Phillips, K. J. H. Et al., *A&A*, **324**, 381 (1997)
26. J. L. R. Saba, et al., *ApJ*, **510**,1064 (1999)
27. E . Takacs et al., manuscript in progress.
28. H.J. Andrä et al., *Z. Phys. D*, **21**, S135 (1991)
29. D. H. Schneider et al., *Radiation and Defects in Solids,* **127**,113 (1993)
30. M. LeGros, et al., *Nucl. Instr. and Meth. in Physics Research*, **A 357**, 110 (1995)
31. J.P. Briand et al., *Nucl. Instr. and Methods*, **B87**, 138 (1994)